FRONTIERS OF PHYSICS

RESEARCH ARTICLE
Volume 18 / Issue 4 / 42302 / 2023

Generation of coherent blue light via bichromatic pumping in cesium vapor

Guiyuan Ge[1], Li Tian[1], Guoqing Zhang[1], Ningxuan Zheng[1], Wenliang Liu[1,2], Vladimir Sovkov[1,3], Jizhou Wu[1,2,5,†], Yuqing Li[1,2], Yongming Fu[4], Peng Li[4], Jie Ma[1,2,5,‡], Liantuan Xiao[1,2], Suotang Jia[1,2]

1 State Key Laboratory of Quantum Optics and Quantum Optics Devices, Institute of Laser Spectroscopy, Shanxi University, Taiyuan 030006, China
2 Collaborative Innovation Center of Extreme Optics, Shanxi University, Taiyuan 030006, China
3 St. Petersburg State University, 7/9 Universitetskaya nab., St. Petersburg 199034, Russia
4 College of Physics and Electronic Engineering, Shanxi University, Taiyuan 030006, China
5 Hefei National Laboratory, Hefei 230088, China
Corresponding authors. E-mail: †wujz@sxu.edu.cn, ‡mj@sxu.edu.cn
Received November 8, 2022; accepted January 10, 2023

ABSTRACT

Diode-pumped alkali lasers, possessing high efficiency and narrow linewidth, can provide feasible solutions for wavelength ranges difficult to reach by commercial lasers. In this study, we investigate a generation of coherent blue light (CBL) via four-wave mixing (FWM)-based up-conversion processes in cesium (Cs) vapor. A bichromatic pumping scheme with 852- and 917-nm lasers drives the Cs atoms to the $6D_{5/2}$ excited level, followed by cascaded decay of $6D_{5/2} \rightarrow 7P_{3/2} \rightarrow 6S_{1/2}$, producing 456-nm CBL under phase matching conditions. The fluorescence in multiple bands from blue to near- and far-infrared in the FWM process is demonstrated under different experimental conditions. To optimize the experimental parameters, we investigate the dependence of 456-nm CBL on the vapor temperature, frequency, and intensity of the two pump lasers. A maximum power of 2.94 mW is achieved with pump powers of 430 mW (for 852 nm) and 470 mW (for 917 nm). The corresponding conversion efficiency is 1.5%/W, three-fold higher than those in previous studies. Our results can contribute to fundamental research on atom–photon interactions and quantum metrology.

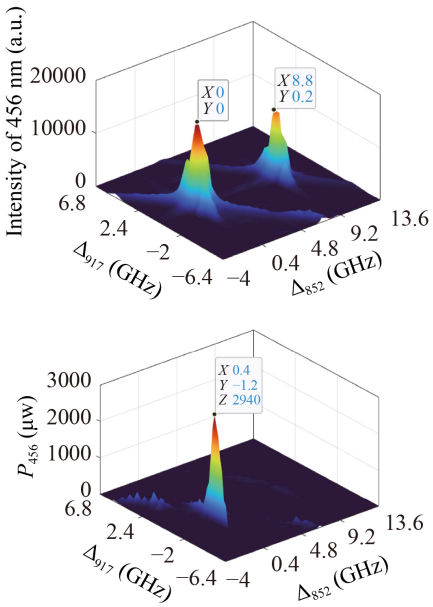

Keywords four wave mixing, conversion, coherent blue beam, bichromatic pumping

1 Introduction

Diode-pumped alkali lasers (DPALs) are renowned for their superior power scalability and beam quality. The usual active medium of DPALs is a vapor of neutral alkali atoms or a mixture of such vapor with buffer gases [1–4]. Diverse combinations of the atomic states of different alkali species results in multiple wavelengths through nonlinear processes [5–8]. Among the various wavelength bands achievable by DPALs, coherent radiation at short wavelengths (e.g., coherent blue light (CBL) or even deep ultraviolet light) is particularly intriguing for its potential applications in quantum information processing, highly sensitive atomic imaging, submarine communications, early detection of rectal cancer, lithography, and optical data storage [9–14].

Higher Education Press

https://doi.org/10.1007/s11467-022-1255-1

DPALs are typically generated by the nonlinear optical effects of parametric four-wave mixing (FWM) and amplified spontaneous emission. The FWM nonlinear process in alkali atoms is a simple and convenient approach to obtain light sources with broad spectroscopic range (from infrared to ultraviolet), low noise level, narrow linewidth, and good beam quality. These properties are naturally inherited from the input near-infrared (NI) pumping lasers. The neutral alkali atoms (Li–Cs: Group 1A elements in the periodic table) are widely employed in CBL generation via FWM nonlinear processes. These metals possess a relatively simple electronic configuration, in which a single s-valance electron exists outside closed s/p-shells [15–18]. Four electronic levels of the alkali atoms, along with three electric-dipole-allowed transitions, are often involved in DPAL applications, such as electromagnetically induced transparency and two-photon absorption [19–22].

Since Krupke *et al.* [23] pioneered the DPAL designs based on NI laser pumping, researchers have generated blue and ultraviolet lights at 456 nm and 459 nm [24, 25], 420 nm [26–28], and 311 nm [29] from Cs, Rb and Na atoms either through two-step excitation using two lasers or two-photon excitation using a single laser. CBLs with powers of tens of μW have been generated in Rb vapor via pumping through the Rb $5S \rightarrow 5P \rightarrow 5D$ transition [26, 30]. In a system with optimized pump polarizations and frequencies, a heated Rb vapor produces high power (1.1 mW) 420-nm CBL, corresponding to a conversion efficiency as high as 260 %/W [27]. Recently, the output power of CBLs generated through the FWM process has been enhanced from tens of μW to the order of mW. These improvements have been enabled by various approaches, such as optimizing the excitation laser frequency [26], introducing an extra seeded laser or repumping laser to repopulate the atoms [24, 25, 33], enlarging the input powers [32], and exerting a ring cavity to increase the cycling strength [6, 28, 31]. These studies have shown that the efficiency of CBL generation is much lower in the Cs species (456 and 459 nm) than in the Rb species (420 nm) because the branching ratio of Rb $5D_{5/2} \rightarrow 6P_{3/2}$ is 35%, whereas that of Cs $6D_{5/2} \rightarrow 7P_{3/2}$ is only 0.4% [17]. Obtaining high-power CBL by the FWM process remains a challenging task in DPAL-related research.

In this work, we report the generation of CBL via FWM-based up-conversion processes in Cs atomic ensemble. Considerably CBL with higher power than previous investigations is achieved by scaling the input bichromatic pumping beams to enough higher power and optimizing their frequency detunings to satisfy the phase matching conditions. We obtain 2.94-mW, 456-nm CBL based on the Cs $6S_{1/2} \rightarrow 6P_{3/2} \rightarrow 6D_{5/2} \rightarrow 7P_{3/2} \rightarrow 6S_{1/2}$ transitions, corresponding to a conversion efficiency $\eta = P_{456}/(P_{852}P_{917})$ of approximately 1.5%/W [34]. The fluorescence in multiple bands (from blue to NI and far-infrared) in the FWM process is also observed. Specifically, we demonstrate the dependences of CBL and fluorescence on the experimental parameters (temperature of the Cs vapor cell, pump laser intensity, and frequency detuning). The saturation effects of the CBL and Autler–Townes (AT) splitting of the excited levels are phenomenologically analyzed. Our investigations are relevant to sensitive atomic and molecular detection, quantum-squeezed and entangled state preparation, and other processes [35–38].

2 Experimental setup

Figures 1(a) and (b) show the experimental setup for generating the 456-nm CBL and the relevant energy levels, respectively. The 852-nm laser beam is served by an external cavity diode laser (ECDL, DL PRO) to drive the Cs D2 $6S_{1/2} \rightarrow 6P_{3/2}$ transition, and the $6P_{3/2} \rightarrow 6D_{5/2}$ transition at 917 nm is induced by a continuous tunable Ti:sapphire laser (MBR-110, linewidth ~ 100 kHz). After injecting through an amplifier (BOOSTA PRO), a maximum of 1.2-W output is achieved for the 852-nm laser. The output power of 0.8 W for the 917-nm laser is obtained by pumping from a diode-pumped solid-state laser (Verdi 10,532 nm, ~ 18 W). The high-power of both lasers helps in investigating the power dependence of CBL generation over a large control range.

The 852-nm light passes via two polarization beam splitters (PBS_1 and PBS_2) to maintain the polarization and change the power. Its frequency is stabilized by the saturated absorption spectrum. An acousto-optic modulator (AOM, MT110-B50A1-IR)-based double-pass configuration is employed to avoid a shift in the position of the diffracted beam and to freely alter the frequency and power of the beam. A telescope system consisting of lenses f_1 and f_2 with focal lengths of 150 mm is designed to improve the AOM diffraction efficiency. By steering mirrors M_1 and M_2, the 852- and 917-nm laser beams well overlap in space and are copropagated via the dichroic mirror (DM, FF880-SDio1-t1) with a transmission efficiency (reflection efficiency) greater than 93.8% (97.7%) for the 852-nm (917-nm) laser beam. The two beams are circularly polarized after passing a quarter-wave plate (QP_2) and converge in the heated Cs vapor cell 1 (length $L = 10$ cm), where they appear at the confocal center of the telescope system f_3–f_4. After optimizing the heating temperature of Cs cell 1,456-nm CBL is generated, and it is detected by a digital optical power meter (PM100D) after passing through a grating (GR13-1205), which disperses the input and output beams from the cell 2. The separated 456-nm blue light then passes through a narrow bandpass filter (FF01-460/14-25) to remove the residual 917- and 852-nm laser beams. Grating spectrometers with sensitivity range of 350–1700 nm are

used to measure the fluorescence at the side of the heating vapor cell 1. The spectra for the produced CBL are recorded by a photodetector after its passing through vapor cell 2.

3 Experimental results and discussion

With 852- and 917-nm pumps, Cs atoms decay to $6S_{1/2}$ through different intermediate levels, causing emissions ranging from blue-violet to near- and mid-infrared (NIR and MIR, respectively) spectral regions. Figure 2(a) shows the fluorescence spectra obtained at powers P_{852} and P_{917} of 430 and 470 mW, respectively, when the Cs vapor cell 1 was heated to 105 ℃. The atomic number density varied from 5.12×10^{12} cm^{-3} to 8.0×10^{13} cm^{-3} as the temperature T varied from 81 ℃ to 129 ℃ in the 100-mm Cs vapor cell 1. Figures 1(b) and 2(b) show the relevant energy levels during Cs atom excitation - deexcitation. Along with the 456-nm blue light, 1359- and 1468-nm MIR light were detected simultaneously from

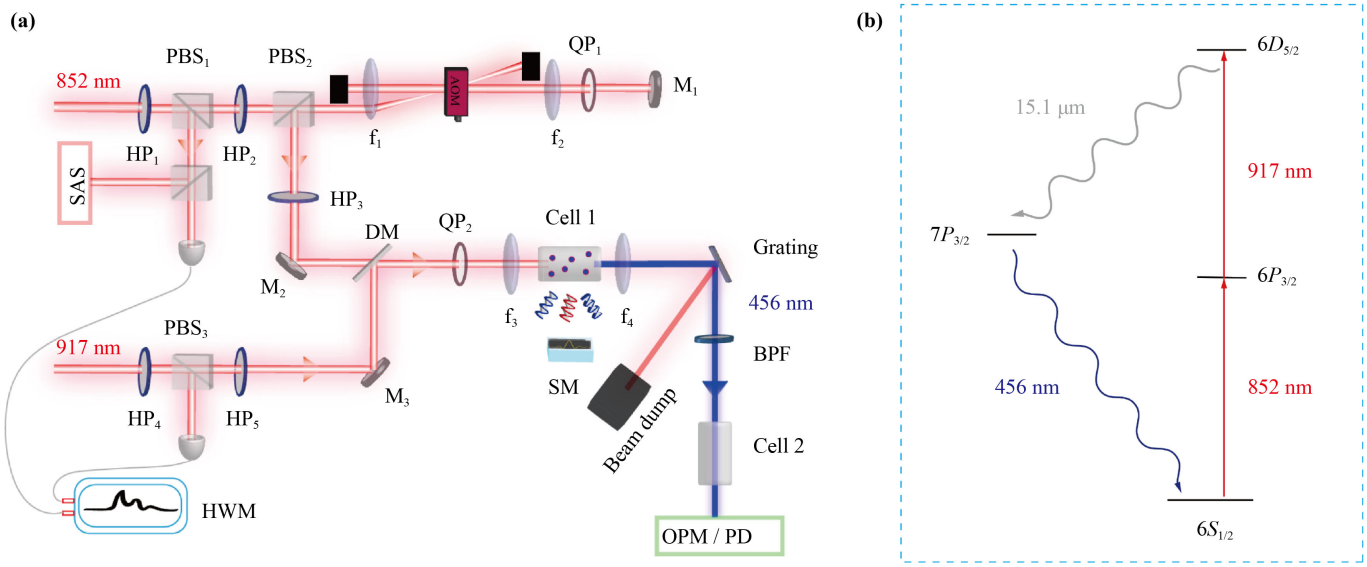

Fig. 1 **(a)** Experimental setup. SAS, saturation absorption spectrum; HP, half-wave plate; PBS, polarization beam splitter; f_1–f_4, focal lenses; QP, quarter wave plate; M, mirror; DM, dichroic mirror; SM, spectrometer; BPF, band pass filter; PD, photodetector; OPM, optical power meter; HWM, high-finesse wavelength meter. **(b)** Relevant energy levels of Cs atoms in this study.

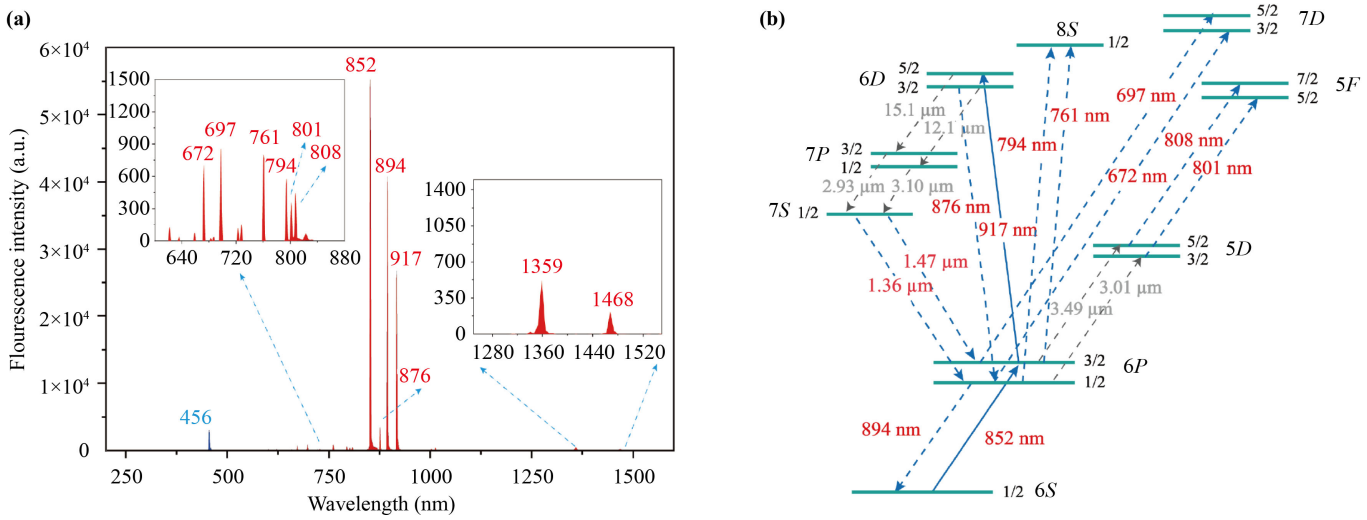

Fig. 2 **(a)** Fluorescence spectra measured at the laser powers P_{852} and P_{917} of 430 and 470 mW respectively, at an optimal vapor cell 1 temperature of 105 ℃. The detunings of the pump light at 852 and 917 nm are set to reach the maximum power of the 456-nm light. Fluorescence with weak signals at 600 nm-850 nm and near-infrared light at 1359 and 1468 nm are zoomed in the insets. **(b)** Relevant energy levels and transitions from red to infrared light.

the spontaneous decay through the channel of the $6D_{5/2} \rightarrow 7P_{3/2} \rightarrow 7S_{1/2} \rightarrow 6P_{3/2}$ (1468 nm) or $\rightarrow 6P_{1/2}$ (1359 nm). Herein, we used a scheme different from those in previous reports [24, 25], where Cs $6D_{3/2}$ was chosen as the excited level to generate two blue lights (455 and 459 nm) in the FWM processes.

Interestingly, in this study, NIR radiations at 876 and 895 nm were also observed, and their fluorescence intensities were much stronger than those of blue light at 456 nm. The 876-nm light, originated from the $6D_{3/2} \rightarrow 6P_{1/2}$ transition, followed by the 895-nm light from the $6P_{1/2} \rightarrow 6S_{1/2}$ transition. However, according to the selection rules, the $6D_{5/2} \rightarrow 6D_{3/2}$ transition is prohibited. Furthermore, as shown in Fig. 2(a), weak fluorescence for shorter wavelengths of 672, 697, 761, 794, 801, and 808 nm, corresponding to the decays from levels higher than $6D_{5/2}$, were also observed. Although these fluorescences appeared as the cell 1 was heated, at these temperatures, only the two lowest hyperfine levels could be noticeably populated at the thermodynamical equilibrium. We assume that step-wise and two-photon processes were triggered during the first excitation step, which generated 456-nm light. During this step, the excitation reached the higher energy levels of Cs atoms and was followed by a cascade of decays [26]. Another possibility is electric-dipole forbidden transitions ($6P_{3/2} \rightarrow 7P_{3/2}$, $6S_{1/2} \rightarrow 6D_{5/2}$) under the high pump power at high temperature [39, 40].

Figures 3(a)–(h) show the relationship between the intensity of the fluorescence at 672, 697, 761, 794, 801, 808, 1359, and 1468 nm and the detuning of the 917-nm pump Δ_{917} at different temperatures for the vapor cell 1. First, regardless of the temperature change, the fluorescence intensity at these wavelengths is always the highest at $\Delta_{917} = -1.2$ GHz. The temperature does not change the detuning of 917 nm at which the fluorescence intensity peak appears. Second, the fluorescence intensity at 672, 697, 761, 794, 801, and 808 nm tends to saturate as the temperature gradually increases to 120 ℃, after which it decreases slowly, as shown in Figs. 3(a)–(f). In contrast, the maximum of fluorescence intensities for 1359 and 1468 nm occurred at 110 ℃, as shown in Figs. 3(g) and (h), followed by a decrease as the temperature keeps rise. A thorough understanding of the spectroscopic properties necessitates a quantitative model considering the dynamics of atoms and the propagation variation of interacting beams.

We measured the relative intensity of the blue fluorescence at 456 nm (using a spectrometer from the side of the cell 1) and the power of the emitted 456-nm CBL (using an OPM after the cell 1) as functions of the detunings Δ_{852} and Δ_{917} of the two pump lasers, as shown in Fig. 4. The frequency of the 852-nm laser was stabilized against $6S_{1/2}(F = 4) \rightarrow 6P_{3/2}(F' = 5)$, while the frequency of the 917-nm laser scanned over the $6P_{3/2} \rightarrow 6D_{5/2}$ transition and vice versa. As shown in Fig. 4(a), the fluorescence intensity demonstrated two peak positions at different detunings, one is resonant for $\Delta_{852} = \Delta_{917} = 0$, and the other $\Delta_{852} = 8.8$ GHz and $\Delta_{917} = 0.2$ GHz. The two ground states ($6S_{1/2}$, $F = 4$ and $F = 3$) of Cs hyperfine structure have both contributed during the cascaded transition. While for the ($F = 3$) state, there is a shift of 0.4 GHz from the hyperfine splitting of 9.19 GHz.

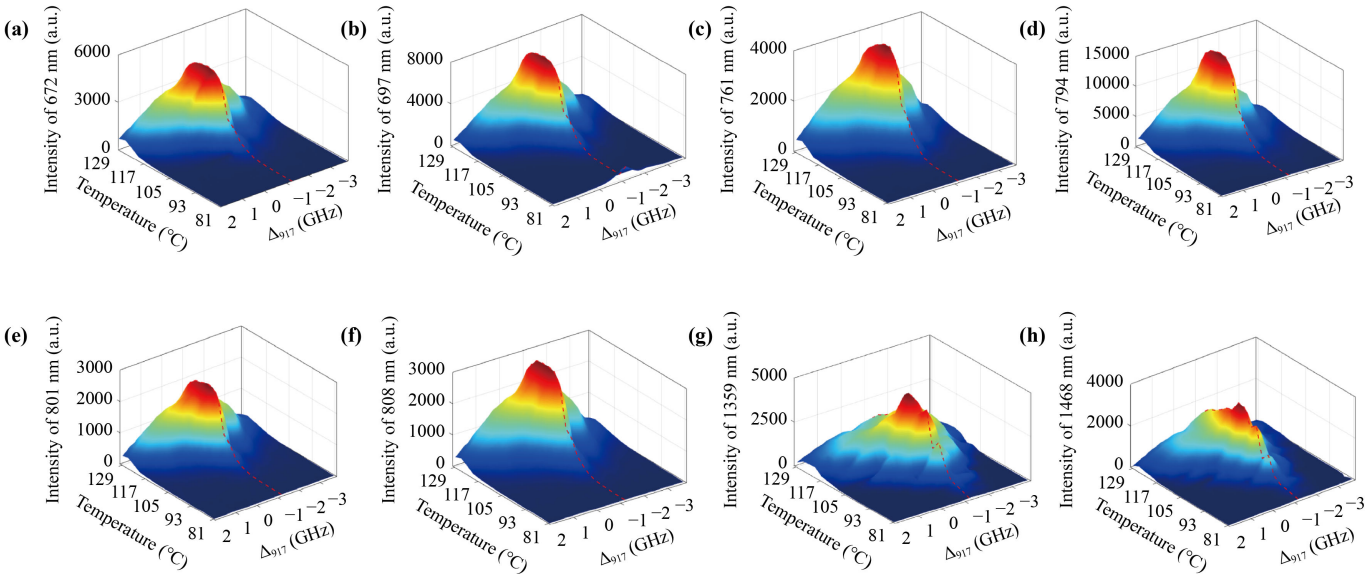

Fig. 3 **(a–h)** Fluorescence intensities at 672, 697, 761, 794, 801, 808, 1359, and 1468 nm as a function of the Cs vapor temperature and pump detuning Δ_{917}. The 852-nm pump light is locked at the optimal position of the fluorescence resonance, and the frequency of the 917-nm pump light sweeps up around $6P_{3/2} \rightarrow 6D_{5/2}$ transition. The origin of the frequency coordinates of 917-nm pump light (917.48850 nm) is at the peak of blue light power.

On the other hand, a maximum power P_{456} = 2.94 mW by satisfying the phase matching relationship $\boldsymbol{k}_{852} + \boldsymbol{k}_{917} = \boldsymbol{k}_{IR} + \boldsymbol{k}_{BL}$, where $\boldsymbol{k}_{852}$, $\boldsymbol{k}_{917}$, $\boldsymbol{k}_{IR}$ and $\boldsymbol{k}_{BL}$ are the wave vectors of 852-nm, 917-nm, 15.1-μm (mid-IR emission light), and 456-nm radiations, respectively. Under the phase matching condition, the detunings of the pump lasers are Δ_{852} = 0.4 GHz and Δ_{917} = –1.2 GHz, as shown in Fig. 4(b). The conversion efficiency of the CBL is $\eta = P_{456}/(P_{852}P_{917}) \sim 1.5\%$/W. The nearly-resonant 852 nm laser efficiently pumped the ground level $6S_{1/2}$ to the intermediate level $6P_{3/2}$, while a proper detuning of the 917 nm laser reduced the atomic absorption for efficient FWM processes under the phase-matching condition [25]. It should be noted that the power of blue light can even be measured (although very weak) at very large detuning range from the resonances of the pump lights. This scenario slightly differs from previous studies [15, 27], in which no CBL appeared under similar conditions. Comparing with the intensity distribution for the fluorescence, the power of CBL has no distribution at Δ_{852} = 8.8 GHz. Actually, the emission into the $6S_{1/2}$ $(F = 4)$ state has a higher transition probability than emission into the $6S_{1/2}$ $(F = 3)$ state, thus the weak emission into the $(F = 3)$ state would be preferentially absorbed in the vapor cell. Table 1 lists the blue CBLs of the 459- and 456-nm CBLs that have so far been acquired in Cs species. In this study, we employed relatively high power for the pump lasers, leading to the broadening of power region of the pump lasers and the obtainment of higher conversion efficiency for the CBL. Comparing with the previous best result [15], the efficiency we achieved is higher by a factor of 3.4.

Figure 5 shows the variation of the CBL power P_{456} with the vapor cell 1 temperature T and the pump powers P_{852} and P_{917}. Figure 5(a) shows the variation of the blue light power at P_{852} = 430 mW and P_{917} = 470 mW with Cs vapor temperature. We conclude that 105 ℃ is the optimal temperature, at which the up-conversion efficiency of the FWM is the highest. When the temperature of the Cs cell rises, the number density of Cs atoms in the cell increases accordingly, further enhancing the CBL power generated by frequency up-conversion. However, at higher temperatures of the vapor cell, the pumped optical power (which is limited) significantly attenuates with increased depth through the atomic medium. As the self-absorption effect of the atomic medium is enhanced, the CBL produced is absorbed by the atomic medium and finally trends downward. At 120 ℃, the blue light power reduced to ~ 10 μW.

Figures 5(b) and (c) show the variation of P_{456} with P_{852} and P_{917} at 105 ℃. As the 852- and 917-nm input powers increased, CBL power saturation was observed at 105 ℃, where the corresponding to an atomic number density of 2.1×10^{13} cm^{-3}. In Fig. 5(b), no blue light was observed below P_{852} = 40 mW, a weak blue light was

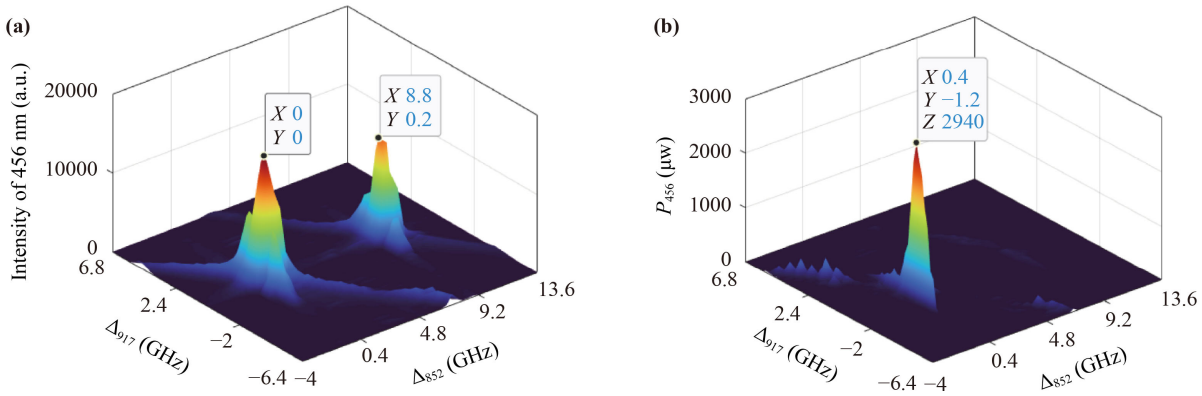

Fig. 4 **(a)** Fluorescence intensity and **(b)** coherent blue light (CBL) power as functions of the pump detunings Δ_{917} and Δ_{852}. The origin of the coordinates in (a) is set at the maximal fluorescence intensity, and the pump wavelengths detected by HWM (WS-U) as 852.35631 and 917.48500 nm.

Table 1 Power P and efficiency η of the CBL generation in Cs atoms via FWM. Other experimental parameters are the pump power P, detuning of pump laser Δ, temperature T, and cell length L.

Ref.	Pump power	Δ_{852}	$\Delta_{917}, \Delta_{921}$	T, L	$P_{CBL,\,\eta}$
[15]	P_{852} = 30 mW P_{917} = 30 mW	0	0	96 ℃ 70 mm	P_{455} = 4 μW (0.44%/W)
[25]	P_{852} = 120 mW P_{921} = 30 mW	0	250 MHz	110 ℃ 30 mm	P_{456} = 15 μW (0.416%/W) P_{459} = 13 μW (0.361%/W)
This work	P_{852} = 430 mW P_{917} = 470 mW	0.4 GHz	–1.2 GHz	105 ℃ 100 mm	P_{456} = 2.94 mW (1.5%/W)

recorded in the range of 40–180 mW, and above 180 mW, it remarkably increased and gradually approached saturation. Similarly as shown in Fig. 5(c), the power of the CBL only increased rapidly as the 917-nm pump power exceeded 100 mW and then slowly approached saturation. The saturation phenomenon of CBL shown has been been reported elsewhere [5, 28, 32, 42]. It is often attributed to the competition between the forward ($6S_{1/2} \rightarrow 6P_{3/2} \rightarrow 6D_{5/2} \rightarrow 7P_{3/2} \rightarrow 6S_{1/2}$) and reverse ($6S_{1/2} \rightarrow 7P_{3/2} \rightarrow 6D_{5/2} \rightarrow 6P_{3/2} \rightarrow 6S_{1/2}$) FWM processes [43]. Moreover, saturation can also be described in terms of the optical depth (OD) of the 852-nm beam [Eq. (1)],

$$OD = N\sigma l, \tag{1}$$

which is a function of the Cs density N, the length l of the Cs vapor cell, and the absorption cross section σ can be calculated as Eq. (2):

$$\sigma = \frac{\sigma_0}{1 + 4(\Delta/\Gamma)^2 + (I/I_{sat})}, \tag{2}$$

where σ_0 is the on-resonance cross section, Δ is the detuning from the resonance, Γ is the spontaneous decay rate, I is the 852 nm laser intensity, and I_{sat} is the saturation intensity of $6P_{3/2}$. The parameters σ_0 and I_{sat} are obtained in the literature [44]. From the blue light saturation intensity of the 852 nm laser, the OD was calculated as $\approx$ 8.1. To better understand and explain the CBL saturation phenomenon, we plan to observe and calculate the OD at different atomic number densities and cell lengths.

At higher light intensity the CBL spectra reveal a doublet structure with the detuning of the 852 nm laser [Fig. 5(d)]. This frequency-dependent splitting suggests that the doublet can be attributed to the Autler–Townes effect. The $6P_{3/2}$ and $6D_{5/2}$ levels were subjected by the high-power 917 nm light, indicating that they were induced through AC-Stark splitting. The CBL peaks occurred as the 852 nm laser light is resonant with the transition from the $6S_{1/2}(F = 4)$ ground state to either ac-Stark split component of the $6P_{3/2}(F = 5)$ level. As the 852 nm laser light is tuned to the cycling transition, the maximum power of CBL occurs with a maximum value of 193 MHz for the splitting, which is larger than those reported in the studies of Rb [26, 45]. The systematic relationship between the power of the 852 nm laser, 917 nm laser and splitting will be investigated in the near future.

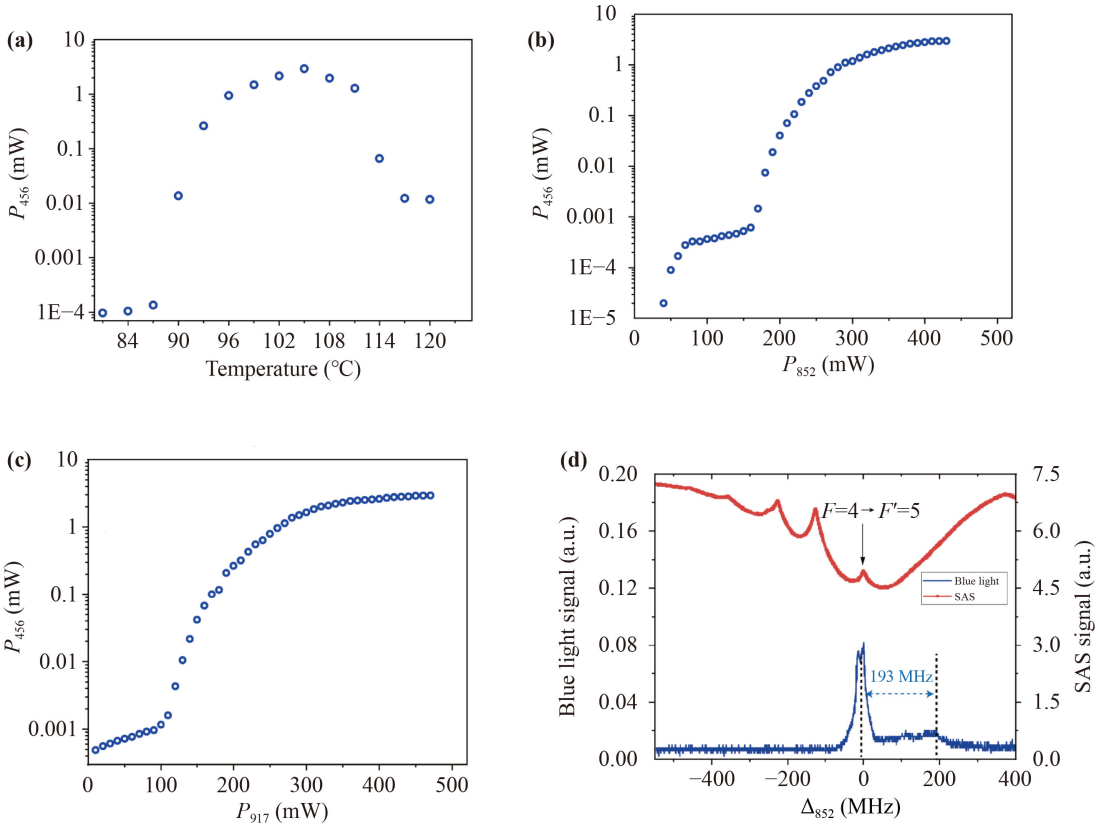

Fig. 5 Power of the emitted 456-nm CBL versus **(a)** temperature of the vapor cell 1 (P_{852} = 430 mW and P_{917} = 470 mW) and **(b, c)** power of the pump laser beams at T = 105 ℃. **(d)** Collimated blue light generated in the Cs cell 1 at 105 ℃ versus the detuning of the 852-nm laser frequency. The 917-nm laser is locked at 917.48850 nm while the 852-nm laser is scanned in the vicinity of the $6S_{1/2}(F = 4) \rightarrow 6P_{3/2}(F' = 5)$.

4 Conclusion

In conclusion, we generated CBL at 456 nm in a hot Cs vapor cell via bichromatic pumping. High-power and frequency-tunable 852- and 917-nm lasers were used to pump Cs atoms to the excited $6D_{5/2}$ level. The maximal output power of the 456-nm CBL (2.94 mW) was achieved with pump lasers tuned to 917.48850 and 852.35728 nm, which satisfies the phase matching conditions. The generation efficiency increased by a factor of 3.4 compared to the best earlier result. NIR coherent emissions at 1359 and 1468 nm were also observed. At the optimal temperature of the Cs vapor and pump power, the power of the generated 456-nm CBL saturated. In the configuration of copropagating optical fields, AT splitting was induced by bichromatic pumping and a large separation (193 MHz) was observed in the doublet structure.

Acknowledgements The authors are grateful to Prof. Jinze Wu from Taiyuan University of Science and Technology for the instructive and fruitful discussions. This work was supported by Innovation Program for Quantum Science and Technology (Grant No. 2021ZD0302100), the National Natural Science Foundation of China (Grants Nos. 62020106014, 62175140, 12034012, 92165106, 12104276, and 62011530047), PCSIRT (No. IRT17R70), 111 Project (Grant No. D18001), the Educational Reform and Innovation Project of Higher education in Shanxi Province (Grant Nos. Z20220001 and Z20220013), the Shanxi 1331 KSC.

References and notes

1. D. D. Xu, F. Chen, J. Guo, M. Z. Shao, and J. J. Xie, Investigation on 447.3 nm blue-violet laser by extra-cavity frequency doubling of a diode-pumped cesium vapor laser, *Opt. Laser Technol.* 83(83), 119 (2016)
2. B. V. Zhdanov, G. Venus, V. Smirnov, L. Glebov, and R. J. Knize, Continuous wave Cs diode pumped alkali laser pumped by single emitter narrowband laser diode, *Rev. Sci. Instrum.* 86(8), 083104 (2015)
3. B. V. Zhdanov, T. Ehrenreich, and R. J. Knize, Highly efficient optically pumped cesium vapor laser, *Opt. Commun.* 260(2), 696 (2006)
4. W. F. Krupke, R. J. Beach, V. K. Kanz, and S. A. Payne, Resonance transition 795-nm rubidium laser, *Opt. Lett.* 28(23), 2336 (2003)
5. A. Akulshin, D. Budker, and R. McLean, Directional infrared emission resulting from cascade population inversion and four-wave mixing in Rb vapor, *Opt. Lett.* 39(4), 845 (2014)
6. R. F. Offer, J. W. C. Conway, E. Riis, S. Franke-Arnold, and A. S. Arnold, Cavity-enhanced frequency up-conversion in rubidium vapor, *Opt. Lett.* 41(10), 2177 (2016)
7. B. Gai, J. Liu, P. Wang, Y. Chen, S. Hu, and J. Guo, Terahertz emitting and four wave mixing details in $6P_{3/2}\rightarrow 11D_J$ pumped cesium vapor, *J. Quant. Spectrosc. Radiat. Transf.* 258, 107351 (2021)
8. B. Gai, S. Hu, J. Chu, P. Wang, X. Cai, and J. Guo, Collimated ultraviolet light generated by four-wave mixing process in Cs vapor, *OSA Continuum* 4(9), 2410 (2021)
9. K. Asano, M. Tsukamoto, Y. Sechi, Y. Sato, S. I. Masuno, R. Higashino, T. Hara, M. Sengoku, and M. Yoshida, Laser metal deposition of pure copper on stainless steel with blue and IR diode lasers, *Opt. Laser Technol.* 107(1), 291 (2018)
10. G. Lu, T. Sakamoto, and T. Kawanishi, Wavelength conversion of optical 64QAM through FWM in HNLF and its performance optimization by constellation monitoring, *Opt. Express* 22(1), 15 (2014)
11. C. Stan-Sion, M. Enachescu, A. R. Petre, M. Duma, D. G. Ghita, G. Kizane, L. Baumane, J. Gabrusenoks, M. Halitovs, L. Avotina, A. Zarins, J. Likonen, S. Koivuranta, and M. Kiisk, Comparison of tritium measurement techniques for a laser cleaned JET tile, *Fusion Eng. Des.* 89(11), 2628 (2014)
12. K. Markowski, Ł. Chorchos, and J. P. Turkiewicz, Influence of four-wave mixing in short- and medium-range 1310 nm dense wavelength division multiplexing systems, *Appl. Opt.* 55(11), 3051 (2016)
13. F. Ali, F. Muhammad, U. Habib, Y. Khan, and M. Usman, Modeling and minimization of FWM effects in DWDM-based long-haul optical communication systems, *Photonic Netw. Commun.* 41(1), 36 (2021)
14. Y. Zhang, F. Zhang, and Y. Bian, Application of laser communication in submarine communication, *Opt. Commun. Tech.* 30(7), 43 (2006)
15. J. T. Schultz, S. Abend, D. Doring, J. E. Debs, P. A. Altin, J. D. White, N. P. Robins, and J. D. Close, Coherent 455 nm beam production in a cesium vapor, *Opt. Lett.* 34(15), 2321 (2009)
16. A. Akulshin, F. Pedreros Bustos, and D. Budker, Intensity-correlated spiking of infrared and ultraviolet emission from sodium vapors, *Opt. Lett.* 46(9), 2131 (2021)
17. O. S. Heavens, Radiative transition probabilities of the lower excited states of the alkali metals, *J. Opt. Soc. Am.* 51(10), 1058 (1961)
18. J. Wu, M. Guo, H. Zhou, J. Liu, J. Li, and J. Zhang, Experimental realization of efficient nondegenerate four-wave mixing in cesium atoms, *Opt. Express* 30(8), 12576 (2022)
19. M. J. Lee, Chen, Y. H. Chen, Wang, I. C. Wang, and I. A. Yu, EIT-based all-optical switching and cross-phase modulation under the influence of four-wave mixing, *Opt. Express* 20(10), 11057 (2012)
20. T. Weeks, S. Wachsmann-Hogiu, and T. Huser, Raman microscopy based on doubly-resonant four-wave mixing (DR-FWM), *Opt. Express* 17(19), 17044 (2009)
21. G. Wang, L. Cen, Y. Qu, Y. Xue, J. H. Wu, and J. Y. Gao, Intensity-dependent effects on four-wave mixing based on electromagnetically induced transparency, *Opt. Express* 19(22), 21614 (2011)
22. M. Yan, E. G. Rickey, and Y. Zhu, Suppression of two-photon absorption by quantum interference, *Phys. Rev. A* 64(4), 043807 (2001)
23. W. F. Krupke, Diode pumped alkali lasers (DPALs) A review, *Prog. Quantum Electron.* 36(1), 4 (2012)

24. Y. Y. Zhang, J. Z. Wu, Y. Y. He, Y. Zhang, Y. D. Hu, J. X. Zhang, and S. Y. Zhu, Observation of the interplay between seeded and self-seeded nondegenerate four-wave mixing in cesium vapor, *Opt. Express* 28(12), 17723 (2020)
25. J. Z. Wu, Y. H. Xu, R. G. Dong, and J. X. Zhang, Experimental realization of wavelength multiplexed nonlinear upconversion in cesium atoms, *Opt. Lett.* 46(13), 3119 (2021)
26. A. M. Akulshin, R. J. McLean, A. I. Sidorov, and P. Hannaford, Collimated blue light generated by four-wave mixing in Rb vapour, *Opt. Express* 17(25), 22861 (2009)
27. A. Vernier, S. Franke-Arnold, E. Riis, and A. S. Arnold, Enhanced frequency up-conversion in Rb vapor, *Opt. Express* 18(16), 17020 (2010)
28. J. P. Yuan, H. Liu, L. R. Wang, L. T. Xiao, and S. T. Jia, Coherent 420 nm light generated by the cavity-enhanced four-wave mixing process in Rb vapor, *Opt. Express* 29(4), 4858 (2021)
29. M. Lam, S. B. Pal, T. Vogt, M. Kiffner, and W. H. Li, Directional THz generation in hot Rb vapor excited to a Rydberg state, *Opt. Lett.* 46(5), 1017 (2021)
30. T. Meijer, J. D. White, B. Smeets, M. Jeppesen, and R. E. Scholten, Blue five-level frequency-upconversion system in rubidium, *Opt. Lett.* 31(7), 1002 (2006)
31. E. Brekke and S. Potier, Optical cavity for enhanced parametric four-wave mixing in rubidium, *Appl. Opt.* 56(1), 46 (2017)
32. J. F. Sell, M. A. Gearba, B. D. DePaola, and R. J. Knize, Collimated blue and infrared beams generated by two-photon excitation in Rb vapor, *Opt. Lett.* 39(3), 528 (2014)
33. J. Z. Wu, M. J. Guo, H. T. Zhou, J. H. Liu, J. H. Li, and J. X. Zhang, Experimental realization of efficient nondegenerate four-wave mixing in cesium atoms, *Opt. Express* 30(8), 12576 (2022)
34. T. Ohtsuka, N. Nishimiya, T. Fukuda, and M. Suzuki, Doppler-free two-photon spectroscopy of $6S_{1/2}$–$6D_{3/2,5/2}$ transition in cesium, *J. Phys. Soc. Jpn.* 74(9), 2487 (2005)
35. Y. Zhang, A. W. Brown, C. Gan, and M. Xiao, Intermixing between four-wave mixing and six-wave mixing in a four-level atomic system, *J. Phys. At. Mol. Opt. Phys.* 40(17), 3319 (2007)
36. L. G. Joneckis and J. H. Shapiro, Quantum propagation in a Kerr medium: Lossless, dispersionless fiber, *J. Opt. Soc. Am. B* 11(1), 150 (1994)
37. A. M. Zheltikov, Phase matching as a gate for photon entanglement, *Sci. Rep.* 7(1), 46115 (2017)
38. M. Matsuura and N. Kishi, High-speed wavelength conversion of RZ-DPSK signal using FWM in a quantum-dot SOA, *IEEE Photonics Technol. Lett.* 23(10), 615 (2011)
39. F. Ramírez-Martínez, F. Ponciano-Ojeda, S. Hernández-Gómez, A. Del Angel, C. Mojica-Casique, L. M. Hoyos-Campo, J. Flores-Mijangos, D. Sahagún, R. Jáuregui, and J. Jiménez-Mier, Electric-dipole forbidden transitions for probing atomic state preparation: The case of the Autler–Townes effect, *J. Phys. At. Mol. Opt. Phys.* 54(9), 095002 (2021)
40. E. A. Chan, S. A. Aljunid, N. I. Zheludev, D. Wilkowski, and M. Ducloy, Doopler-free approach to optical pumping dynamics in the $6S_{1/2}$–$5D_{5/2}$ electric quadrupole transition of cesium vapor, *Opt. Lett.* 41(9), 2005 (2016)
41. A. Akulshin, C. Perrella, G. Truong, R. McLean, and A. Luiten, Frequency evaluation of collimated blue light generated by wave mixing in Rb vapour, *J. Phys. At. Mol. Opt. Phys.* 45(24), 245503 (2012)
42. E. Brekke and N. Swan, Saturation and alternate pathways in four-wave mixing in rubidium, *J. Opt. Soc. Am. B* 36(2), 421 (2019)
43. R. K. Wunderlich, W. R. Garrett, R. C. Hart, M. A. Moore, and M. G. Payne, Nonlinear optical processes near the sodium 4D two-photon resonance, *Phys. Rev. A* 41(11), 6345 (1990)
44. D. A. Steck, Webpage: steck.us/alkalidata, Revision 2.1.6, 20 September, 2013
45. M. P. Moreno, A. A. C. de Almeida, and S. S. Vianna, Interference effect and Autler–Townes splitting in coherent blue light generated by four-wave mixing, *Phys. Rev. A* 99(4), 043410 (2019)